Quantifying the contribution of Fc-mediated effector functions to the antiviral activity of anti–HIV-1 IgG1 antibodies in vivo

Pengfei Wang[a], Mili R. Gajjar[a], Jian Yu[a], Neal N. Padte[a], Agegnehu Gettie[a], James L. Blanchard[b], Kasi Russell-Lodrigue[b], Laura E. Liao[c], Alan S. Perelson[c], Yaoxing Huang[a], and David D. Ho[a,1]

[a]Aaron Diamond AIDS Research Center, Columbia University Vagelos College of Physicians and Surgeons, New York, NY 10032; [b]Tulane National Primate Research Center, Tulane University, Covington, LA 70433; and [c]Theoretical Biology and Biophysics, Los Alamos National Laboratory, Los Alamos, NM 87545

Edited by Stephen P. Goff, Columbia University Medical Center, New York, NY, and approved June 17, 2020 (received for review April 27, 2020)

In combating viral infections, the Fab portion of an antibody could mediate virus neutralization, whereas Fc engagement of Fc-γ receptors (FcγRs) could mediate an array of effector functions. Evidence abounds that effector functions are important in controlling infections by influenza, Ebola, or HIV-1 in animal models. However, the relative contribution of virus neutralization versus effector functions to the overall antiviral activity of an antibody remains unknown. To address this fundamental question in immunology, we utilized our knowledge of HIV-1 dynamics to compare the kinetics of the viral load decline (ΔVL) in infected animals given a wild-type (WT) anti–HIV-1 immunoglobulin G1 (IgG1) versus those given a Fc-Null variant of the same antibody. In three independent experiments in HIV-1–infected humanized mice and one pivotal experiment in simian–human immunodeficiency virus (SHIV)-infected rhesus macaques, an earlier and sharper decline in viral load was consistently detected for the WT antibody. Quantifications of the observed differences indicate that Fc-mediated effector functions accounted for 25–45% of the total antiviral activity in these separate experiments. In this study, Fc-mediated effector functions have been quantified in vivo relative to the contribution of virus neutralization mediated by the Fab.

antibody | effector functions | neutralization | HIV-1 dynamics | in vivo quantification

There is an abundance of evidence demonstrating the importance of Fc-mediated effector functions to the overall activity of an antibody in vivo (1–3). In combating viral infections, the Fab portion of an antibody could mediate virus neutralization, whereas Fc engagement of FcγRs could mediate an array of effector functions, including 1) enhanced clearance of virus particles by cells, such as hepatic Kupffer cells, 2) improved adaptive immunity due to "vaccinal effects" of antigen presentation by dendritic cells, and 3) more effective killing of virus-infected cells. The latter may be mediated by antibody-dependent cellular cytotoxicity (ADCC), antibody-dependent cellular phagocytosis (ADCP), and complement-dependent cytotoxicity (1, 2). Natural killer (NK) cells are believed to be the principal mediator of ADCC along with macrophages and neutrophils (1, 4–6). On the other hand, macrophages and neutrophils are thought to be significant players in ADCP (1, 6).

Nature has created an elaborate array of FcγRs for a good reason, and the importance of effector functions mediated by these receptors has been clearly and abundantly established in several animal models of viral infections. For passively administered anti-stalk monoclonal antibodies (mAbs) with modest virus-neutralizing activity, Fc engagement of FcγRs led to improved protection against influenza infection in mice (7). Similarly, systematic evaluations of two large panels of mAbs directed to the Ebola virus glycoprotein showed that effector functions do, indeed, contribute to protection in mice (8, 9). Specifically, virus-neutralizing activity in vitro was not always predictive of protection in vivo, and, in fact, a number of nonneutralizing antibodies conferred protection in mice presumably via effector functions.

In the HIV/AIDS field, the importance of the Fc-mediated effector function in vivo was first shown by Hessell and colleagues (10), who reported that passive administration of a virus-neutralizing mAb, b12 (11–13), protected macaques against SHIV challenge, but this protective effect was partially lost when effector functions were knocked out by the Leu234Ala/Leu235Ala (LALA) mutations (10, 14). Interestingly, ablating complement binding had no adverse impact on the protective effect of b12. More recently, a similar study using a broadly neutralizing mAb (bNAb) PGT121 did not show a loss of protection against SHIV challenge in macaques when the LALA mutations were introduced into its Fc (15). While seemingly contradictory, it is possible that any contribution of effector functions in the latter study was obscured by the high neutralization potency of PGT121. Studies of bNAbs in mouse models have also demonstrated the importance of antibody effector functions. Treatment of acutely infected humanized mice with antiretroviral therapy (ART) plus a mixture of bNAbs and a mixture of latency reversal agents led to a reduced frequency or a delay in viral rebound after all interventions were removed (16). Interestingly, the beneficial antiviral effect was partially lost when the bNAbs were substituted by antibody variants devoid of Fc effector functions. Indeed, 3BNC117 (17), a well-known bNAb, has been shown to suppress HIV-1 better in humanized mice when

Significance

Virus-neutralizing monoclonal antibodies have been tested for the treatment or prevention of HIV-1 infection. Such an antibody can block virus infectivity and mediate killing of virus-infected cells by Fc-mediated effector functions. The relative contributions of these two antibody activities in vivo have not been quantified previously. By quantitatively analyzing results from experiments conducted in HIV-1–infected humanized mice and SHIV-infected rhesus macaques, we have determined that Fc-mediated effector functions contribute about 25–45% to the total antiviral activity of the anti–HIV-1 monoclonal antibodies tested.

Author contributions: P.W. and D.D.H. designed research; P.W., M.R.G., J.Y., A.G., J.L.B., K.R.-L., and Y.H. performed research; P.W., N.N.P., L.E.L., A.S.P., and D.D.H. analyzed data; P.W. and D.D.H. wrote the paper; and N.N.P. performed project management.

Competing interest statement: J.Y., Y.H., and D.D.H. are inventors on a patent describing 10E8.2/iMab and 10E8.4/iMab. D.D.H. is the scientific founder of TaiMed Biologics, Inc., which is focused on antibody therapies for HIV/AIDS.

This article is a PNAS Direct Submission.

[1]To whom correspondence may be addressed. Email: dh2994@cumc.columbia.edu.

This article contains supporting information online at https://www.pnas.org/lookup/suppl/doi:10.1073/pnas.2008190117/-/DCSupplemental.

First published July 14, 2020.

its Fc could engage activating FcγRs (18). Moreover, another study found that the number of ex vivo HIV-1–infected cells injected into the spleen of immunodeficient mice was reduced twofold more by 3BNC117 with a WT Fc as compared to the Fc-Null variant (19).

There are also clinical suggestions of a protective role for Fc-mediated effector functions in HIV-1 infection in humans. For example, high levels of virus-specific ADCC in the patient serum/plasma have been 1) correlated with slower disease progression (20–22), 2) shown to play a role in controlling HIV-1 infection in elite controllers (23), and 3) implicated as an immune correlate of the modest protection observed in the RV144 vaccine trial (24, 25).

Taken together, the one PGT121 study notwithstanding (15), there is an overwhelming abundance of evidence demonstrating that Fc-mediated effector functions are crucial in fighting virus infections in vivo. What then is the extent of their importance? How much do they contribute to the overall activity of an antiviral antibody? What are the relative contributions of the Fab (virus neutralization) versus Fc (effector functions)? This basic issue, posed by the questions above, has yet to be addressed by experimentation to date. To answer these fundamental questions in immunology, we started to utilize our knowledge of HIV-1 dynamics to quantify effector functions of anti–HIV-1 antibodies in vivo.

We and others showed long ago that HIV-1 particles and productively infected CD4 T cells in infected persons turn over rapidly with a combined $t_{1/2}$ of <2 d (26, 27). Our group went on to tease out the details by fitting patients' plasma ΔVL following ART to the mathematical equations that describe the dynamics of each of these two populations (*SI Appendix*, Fig. S1). That plasma virions have a $t_{1/2}$ of ∼45 min and that productively infected CD4 T cells have a $t_{1/2}$ of ∼0.7 d were remarkably consistent among dozens of HIV-1–infected patients studied (28–32). ART only blocked de novo infection (rendering virion infectivity k to or near 0) but had no effect on the death rate of productively infected CD4 T cells δ. As we shifted the analyses to measure the antiviral effects of anti–HIV-1 antibodies, we recognized that an antibody lacking Fc-mediated effector functions would behave similarly to ART, whereas a WT antibody could have an additional impact on δ. Moreover, the binding of antibody–virus complexes to FcγRs could facilitate the rate of particle removal c. Therefore, the expectation is that the plasma ΔVL should begin earlier, and its overall exponential decay slope, corresponding to δ, should be larger when effector functions are substantially contributory. We then used this approach to quantify the relative contributions of virus neutralization versus effector functions of anti–HIV-1 IgG1s in two different experimental animal models.

Results

In Vitro Characterization of Antibodies. The first antibody chosen for study is an anti–HIV-1-Env-bispecific antibody, termed 117/1,400, with one arm composed of 3BNC117 (17) directed to the CD4-binding site on gp120 and the other arm composed of PGDM1,400 (33) directed to the V2/apex region of the envelope spike (*SI Appendix*, Fig. S2*A*). It was constructed using the CrossMAb technology as previously described (34) and engineered to have human IgG1 Fc. This bispecific antibody showed potent and broad neutralization against a panel of 118 HIV-1 strains in vitro (*SI Appendix*, Fig. S2*B*). We also created a Fc-Null variant of 117/1,400 by introducing L234F, L235E, and P331S (collectively known as TM) mutations as well as the N297A mutation that are known to abolish all Fc-mediated effector functions (35, 36). Both WT and Fc-Null variants of 117/1,400 were made as quality products (*SI Appendix*, Fig. S2*C*) and shown to have nearly identical in vitro neutralization profiles against HIV-$1_{JR\text{-}CSF}$ (*SI Appendix*, Fig. S2*D*). As expected, 117/1,400-WT bound all human FcγRs tested, whereas 117/1,400-Null did not (*SI Appendix*, Fig. S2*E*). These results indicate that the WT and Null variants differ only in their binding to FcγRs.

Quantifying Antibody Effector Functions in HIV-1–Infected Humanized Mice. For our initial study, we used a humanized mouse model of HIV-1 infection to assess viral dynamics following administration of 117/1,400-WT or 117/1,400-Null. Immunodeficient NOD/SCID/IL2rγ^{null} (NSG) mice were reconstituted with human hematopoietic stem cells and then infected with HIV-$1_{JR\text{-}CSF}$ as reported previously (34). Once steady-state viremia was reached (*SI Appendix*, Fig. S3), these animals were divided into two comparable groups (*SI Appendix*, Table S1, first experiment). One group received 117/1,400-WT (2.5 mg/mouse, intraperitoneal [i.p.] injection), and the other group received 117/1,400-Null (identical dose and route). To avoid the emergence of resistant viruses that could confound our viral dynamic analyses, we added another bispecific antibody 10E8.2/iMab (ref. (34), $10E8_{V2.0}$/iMab) to both groups. Note that this second bispecific antibody is devoid of effector functions due to the presence of TM and N297A mutations. Subsequently, blood was collected from each mouse serially for 5 d to determine the changes in plasma viral load by RT- PCR. We focused on this time period because our prior knowledge of HIV-1 dynamics suggested that these data points would be most informative in assessing the rapid first phase decay (27, 28, 30–32) and would minimize the second phase effects that could emerge after day 5 posttreatment (28).

The results of viral load changes are shown in Fig. 1*A*. It was discernible that the viral decay slopes for mice receiving 117/1,400-WT were, indeed, steeper than those for mice receiving the Fc-Null variant. Moreover, this visual impression was confirmed by calculating each decay slope, and, strikingly, the top six largest decay slopes were all found in the WT group (Fig. 1*A*). This difference in decay slopes was not related to pharmacokinetics (PK) differences of the two antibody variants. In fact, 117/1,400 levels were slightly lower for the WT group, while 10E8.2/iMab levels were quite similar (*SI Appendix*, Fig. S2*F*). These results were an early indicator that effector functions do, indeed, contribute to the antiviral activity of an antibody in vivo.

Next, we repeated this mouse experiment to seek confirmation. In addition, we assessed if effector functions can be enhanced by introducing the GASDALIE mutations that purportedly increased the binding to human FcγRs (37). This new variant of 117/1,400 was also found to be of good quality and demonstrated nearly identical in vitro neutralization of HIV-$1_{JR\text{-}CSF}$ (*SI Appendix*, Fig. S2 *C* and *D*). Indeed, 117/1,400-GASDALIE had better binding to FcγRs (*SI Appendix*, Fig. S2*E*). We then performed an experiment with five HIV-$1_{JR\text{-}CSF}$-infected humanized mice given 117/1,400-WT, four given 117/1,400-Null, and four given 117/1,400-GASDALIE (*SI Appendix*, Table S1, second experiment). A dose of 2.5 mg was administered i.p. to each mouse. As shown in Fig. 1*B*, the viral decay slopes were again noticeably sharper for the WT group compared to the Null group, despite having similar serum antibody levels (*SI Appendix*, Fig. S2*G*). This conclusion is, likewise, supported by rank order analysis of decay slopes. The GASDALIE variant only yielded decay slopes marginally greater than those observed for the WT antibody (Fig. 1*B*).

We further analyzed the results of these two experiments but did so separately because the two sets of mice were humanized using different fetal livers. In the first study, the mean decay slopes were −0.87/d for the WT group and −0.65/d for the Null group, a difference that reached statistical significance (Fig. 1*C*). In the second study, the mean slopes were −0.66/d for the WT group, −0.36/d for the Null group, and −0.78/d for the GASDALIE group (Fig. 1*D*). Again, the difference between WT and Null groups was statistically significant, whereas the difference between WT and GASDALIE groups was not. The latter suggested that the gain in effector function from GASDALIE mutations was, at best, marginal at the dose tested. We then took

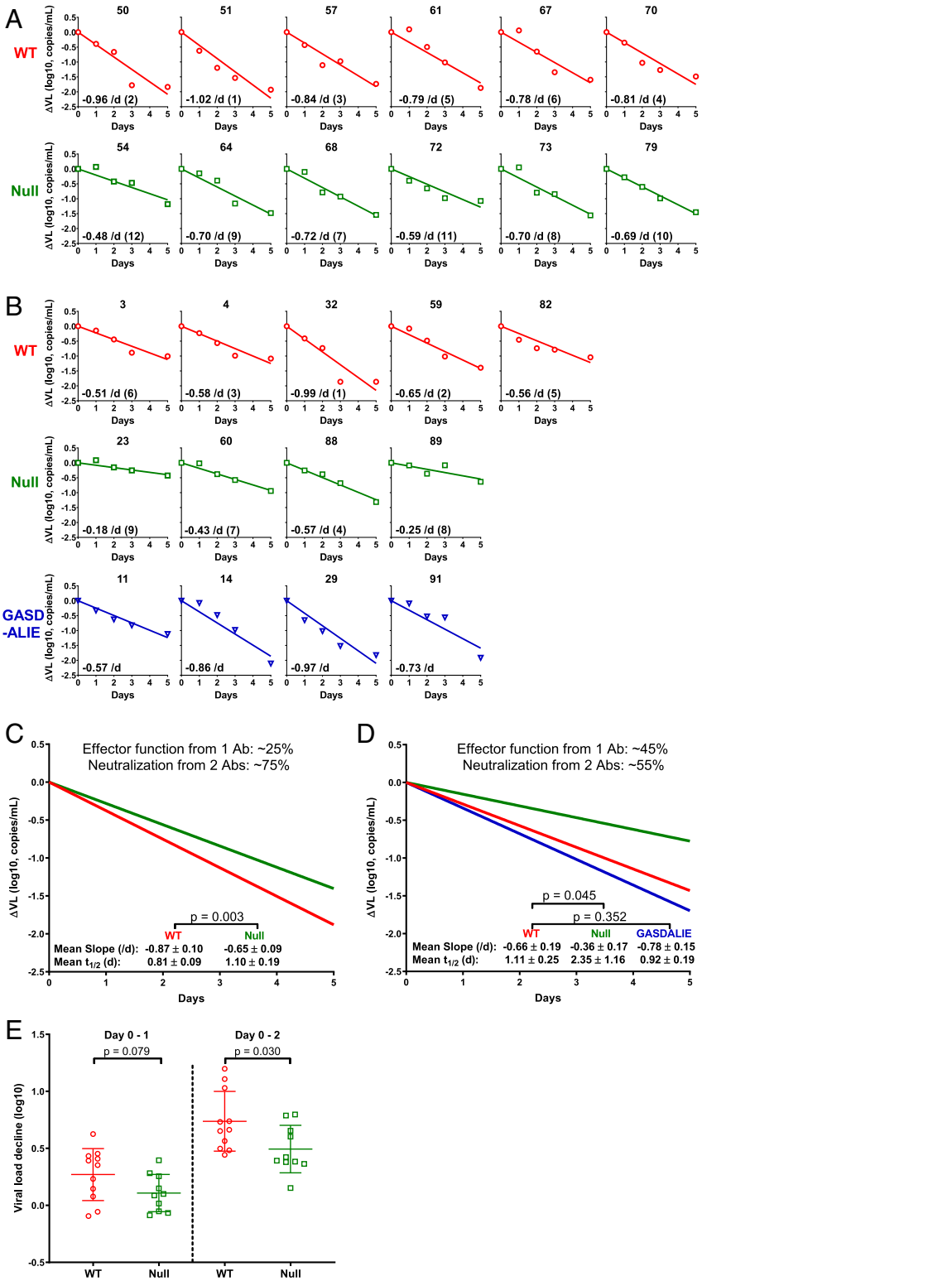

Fig. 1. Measuring and analyzing the decline in plasma viral load in HIV-1-infected humanized mice following administration of 117/1,400 variants. (*A* and *B*) HIV-$1_{JR\text{-}CSF}$-infected humanized mice were treated with 117/1,400-WT (red), 117/1,400-Null (green), or 117/1,400-GASDALIE (blue). Plasma ΔVL is shown for each individual mouse. The decay slope (per day), calculated on a natural log scale, is also shown as an *Inset* in each panel followed by the rank order for the decay slopes in parentheses (1 being the largest and 12 being the smallest, comparing WT to Null only). (*C* and *D*) Mean decay slopes for the WT group (red) and Null group (green) in the first (*C*) and second (*D*) experiments with the latter also showing the mean decay slope for the GASDALIE group (blue). The relative contribution of Fc-mediated effector functions was computed as the difference in slope between WT and Null divided by the WT slope. (*E*) Magnitude of plasma ΔVL from both mouse experiments combined from day 0–1 and day 0–2 postantibody treatment. Lines represent mean ± SD, and *P* values were calculated by a two-tailed *t* test.

the slope of the WT group as indicative of the antiviral effect mediated by the neutralizing activities of two antibodies (117/1,400 and 10E8.2/iMab) plus the effector functions of one (117/1,400) and the slope of the Null group as indicative of the effect of the two neutralizing antibodies without any effector functions. Thus, by simple subtraction, the difference provides a numerical estimate for the magnitude of the contribution of effector functions of 117/1,400-WT in vivo: 25% in the first experiment and 45% in the second experiment (Fig. 1 *C* and *D*).

The early impact of effector functions by 117/1,400-WT was also evident by analyzing the drop in viral load between day 0 and 1 when blocking de novo infection only (by ART or Fc-Null antibody) should have no impact since its suppressive effect would not emerge until one viral generation later (32). As shown in Fig. 1*E*, the mean decrease for mice treated with 117/1,400-WT in the two experiments was 0.3 log, which was not significantly greater than the mean decrease of 0.1 log for 117/1,400-Null. Previous dynamics studies in humans showed that blocking de novo infection resulted in no decline in plasma viral load until after 30 h following ART administration, and a meaningful decline typically began only after 36 h (32). Since we do not have a data point at day 1.5, we also analyzed the decline between day 0 and day 2 as a surrogate. The mean decline was, indeed, significantly greater for the WT group than the Null group (Fig. 1*E*), an early indicator of effector functions at work.

Quantifying Antibody Effector Functions in SHIV-Infected Rhesus Macaques. A humanized mouse is far from being a normal animal. It is deficient in murine T and B cells. Although it has human CD4 and CD8 T cells, its NK cell number and function are grossly abnormal (38). It does have murine macrophages, which may have played a role in mediating effector functions, such as ADCC and ADCP, in the above mouse studies. However, it is a stretch to extrapolate findings and conclusions from such a model system to a normal animal or human. We, therefore, extended our studies to SHIV-infected monkeys. Ample evidence supports the use of rhesus macaques to interrogate the effector functions of human antibodies. Both species have four IgG subclasses with IgG1 being the most important (39), and structural studies show that human and rhesus IgG1 bind FcγRs in similar ways (40). Furthermore, the distribution and expression of rhesus FcγRs are comparable to those observed in key human cell populations, such as NK cells and macrophages (41).

Twelve rhesus macaques were infected with SHIV.A.BG505 (42) until steady-state viremia was reached at week 8 (*SI Appendix*, Fig. S4*A*) and then divided into two equal groups with comparable baseline characteristics (*SI Appendix*, Table S2). One group was given 117/1,400-WT and another was given 117/1,400-Null. Both antibody variants were made as quality products that showed similar neutralization profiles against SHIV.A.BG505 (*SI Appendix*, Fig. S4 *B* and *C*). Again, the only disparity was their binding to rhesus FcγRs (*SI Appendix*, Fig. S4 *D* and *E*). A second Fc-Null antibody (10E8.4/iMab) (43), instead of 10E8.2/iMab (34), was administered to preclude the emergence of resistant virus that may confound the interpretation of results. Each antibody was administered intravenously (i.v.) at a dose of 10 mg/kg, and blood was frequently sampled following a schedule (*SI Appendix*, Fig. S4*A*) that recapitulated what was performed previously in HIV-1-infected patients (32).

As shown in Fig. 2*A*, a precipitous decline in plasma viral load was observed for each monkey, but the decay slopes were larger for monkeys receiving 117/1,400-WT than those receiving 117/1,400-Null, despite similar antibody PK profiles (*SI Appendix*, Fig. S4*F*). The mean decay slope for the WT group was −0.68/d, which was significantly higher than the mean of −0.47/d for the Null group (Fig. 2*B*). Calculations based on these results indicated that 31% of the overall antiviral activity in the macaques was attributable to the effector functions of 117/1,400-WT. While using simianized antibodies could have minimized immunogenicity as a potential confounder in the monkey studies, our experimental data showed that anti-antibody responses were not detectable until day 10 (*SI Appendix*, Fig. S4 *G* and *H*). Thus, our analyses focused on the first 5 d postantibody administration should not be adversely affected.

We further analyzed the drop in plasma viral load from day 0 to day 1.5. As shown in Fig. 2*C*, no noticeable effect (mean 0.0 log) was observed in macaques receiving 117/1,400-Null, exactly as we reported for patients starting ART to block de novo infection (32). In contrast, the drop for macaques treated with 117/1,400-WT was significantly greater (mean 0.4 log). This early measurable impact of the WT antibody cannot be due to virus neutralization for reasons discussed above but is likely indicative of killing of productively infected cells mediated by mechanisms, such as ADCC or ADCP. We also noted a discernible but transient ΔVL at 8 h postadministration of the WT antibody (Fig. 2*C*). Faster virion clearance may be an explanation, but it is unclear why such an effect would be so transient that it is no longer detectable at 16–24 h. Additional studies are needed to verify and explain this acute change.

Given the importance of this macaque experiment, we looked for another independent measure of the impact of effector functions mediated by 117/1,400-WT. We, therefore, quantified SHIV-1 RNA in serial peripheral blood mononuclear cell (PBMC) samples collected from both groups of animals. As shown in Fig. 3, not much difference was observed in the first 3 d, but the subsequent decrease was greater for the group treated with the WT antibody. Using linear regression, we fitted a line through all of the data for each group and found that the mean decay slope for the WT group (−0.54/d) was, again, significantly larger than for the Null group (−0.18/d). Given the lack of prior experience in using cell-associated viral RNA to interpret HIV-1 dynamics, we are reluctant to draw quantitative conclusions therefrom. Instead, we used the results of Fig. 3 as a qualitative confirmation of the conclusions already reached.

Quantifying Antibody Effector Functions with a Different Virus and a Different Antibody. Next, we repeated the antibody/viral dynamics experiment with a different virus and a different antibody to ensure that our results and conclusions are not limited to a "n" of 1. Humanized mice infected with HIV-$1_{pNL(AD8)}$ were used, and the antibody chosen was N6-LS, targeting the CD4-binding site on gp120 (44). N6-LS-WT was provided to us by J. Mascola of NIH, and the Null antibody was generated in-house by introducing the TM and N297A mutations. Both variants were of good product quality and showed similar in vitro neutralization activity against HIV-$1_{pNL(AD8)}$ (*SI Appendix*, Fig. S5 *A* and *B*). However, the WT variant bound FcγR, whereas the Null variant did not (*SI Appendix*, Fig. S5*C*). The infected humanized mice were again divided into two comparable groups (*SI Appendix*, Table S1, third experiment) with one group given N6-LS-WT and the other group given N6-LS-Null. A dose of 2.5 mg was administered i.p. to each mouse. As shown in Fig. 4 *A* and *B*, the slopes of the plasma ΔVL were larger for mice treated with N6-LS-WT (mean −0.60/d) compared to slopes for mice treated with N6-LS-Null (mean −0.37/d), despite having similar antibody PK (*SI Appendix*, Fig. S5*D*). We then calculated the contribution of effector functions to the total antiviral activity of N6-LS-WT to be 39% (Fig. 4*B*). The immediate impact on plasma viral load in the first 36 h was again observed for the WT group only (Fig. 4*C*), once more indicating the presence of an antiviral effect beyond virus neutralization.

Discussion

In four separate experiments in infected humanized mice and rhesus macaques, we have determined the contribution of Fc-mediated effector functions to the overall activity of two IgG1 antibodies against two strains of HIV-1 and one strain of SHIV

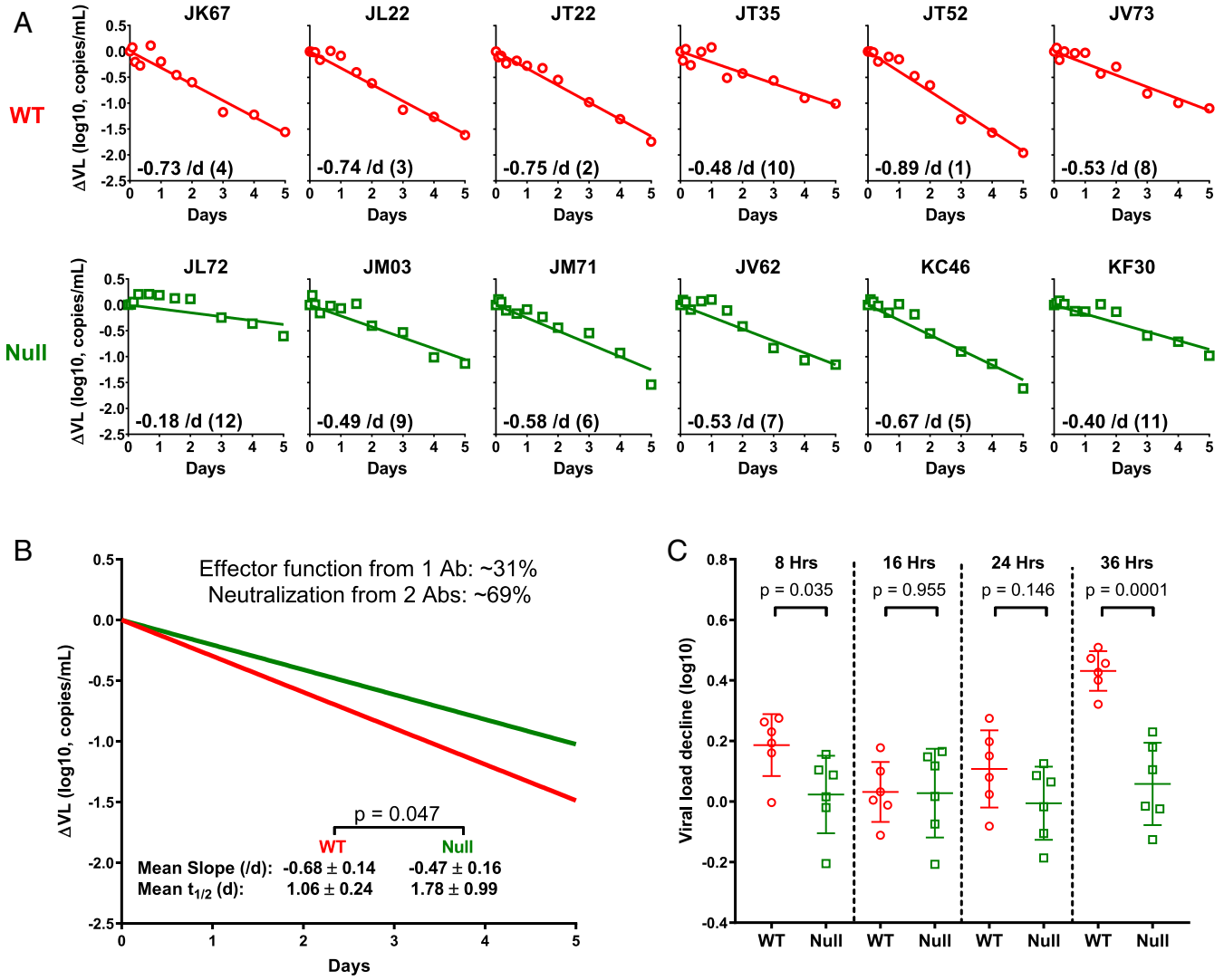

Fig. 2. Measuring and analyzing the decline in plasma viral load in SHIV-infected rhesus macaques following administration of 117/1,400-WT or 117/1,400-Null. (*A*) SHIV.A.BG505-infected rhesus macaques were treated with 117/1,400-WT (red) or 117/1,400-Null (green). Plasma ΔVL is shown for each monkey. The decay slope, calculated on a natural log scale, is also shown as an *Inset* in each panel along with its rank order. (*B*) Mean decay slopes for the WT and Null groups. (*C*) Magnitude of plasma ΔVL from 0–8, 16, 24, and 36 h postantibody treatment. Lines represent mean ± SD, and *P* values were calculated by a two-tailed *t* test.

to be in the range of 25–45%. In particular, the first two experiments in HIV-$1_{JR\text{-}CSF}$–infected humanized mice yielded values of effector function contribution of 117/1,400-WT to be 25% and 45% in the context of virus neutralization mediated by two antibodies (Fig. 1 *C* and *D*). The pivotal experiment in SHIV.A.BG505-infected macaques yielded a value of 31% for 117/1,400-WT, again, in the context of antibody neutralization mediated by two antibodies (Fig. 2*B*). Lastly, in the final study in HIV-$1_{pNL(AD8)}$–infected humanized mice, the effector function was measured on a single mAb (N6-LS) and found to be 39% (Fig. 4*B*). Nevertheless, all four animal studies also showed that the dominant antiviral effect of the antibodies tested was virus neutralization that prevented new rounds of infection. We are able to reach these quantitative conclusions because prior studies of HIV-1 dynamics in infected humanized mice (18, 45) and SIV or SHIV dynamics on infected rhesus macaques (46–48) have been found to be similar to that reported for HIV-1 dynamics in patients.

Our experimental design does not allow us to identify the specific effector functions responsible for the added antiviral activity nor the precise cell populations involved. However, the finding of substantial effector functions in humanized mice known to have NK cells that are inadequate in numbers and functions (38, 49) does suggest that perhaps murine macrophages and/or neutrophils may play an important role in mediating cytotoxicity against cells infected by HIV-1. Overall, our quantitative findings are largely in agreement with published reports demonstrating the importance, qualitatively, of effector functions of anti–HIV-1-Env antibodies in vivo (10, 14, 16, 18, 19). A recent study failed to detect any impact of effector functions on SHIV infection in vivo, but its conclusion was confounded by inadequate antibody dosing and emergence of antibody-resistant virus (15). We fully expect the contribution of Fc-mediated effector functions to vary for each antibody or virus studied experimentally. Nevertheless, our viral dynamics approach establishes a new paradigm to interrogate further the relative importance of an array of antiviral functions mediated by an antibody, including the identification of the role of key cell populations responsible for antibody-mediated effector functions.

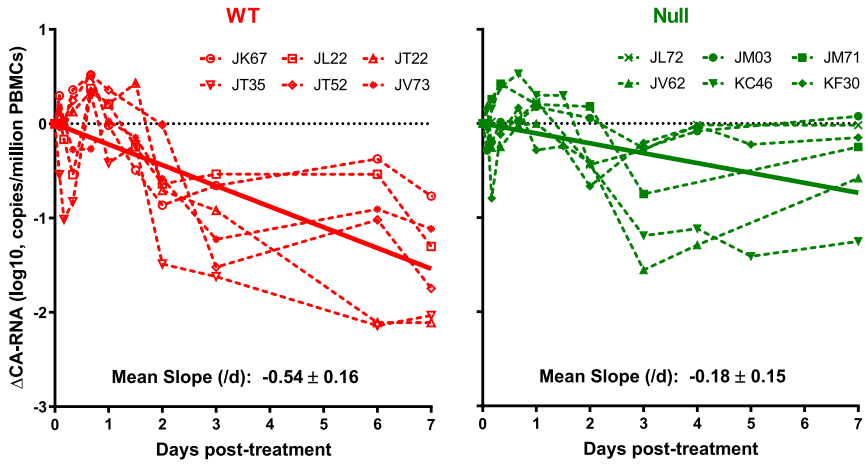

Fig. 3. Measuring and analyzing the decline in cell-associated SHIV RNA in serial PBMC samples from macaques treated with 117/1,400-WT (red) or 117/1,400-Null (green). Each dashed line represents the changes measured in an animal, whereas the dark solid lines represent the best-fit line from linear regression analysis of all of the data for each group. The mean slopes, calculated on a natural log scale for these two best-fit lines, are significantly different (−0.54/d versus −0.18/d) with a *P* value of 0.004.

Materials and Methods

Reagents. HIV-$1_{JR\text{-}CSF}$, HIV-$1_{pNL(AD8)}$, and TZM-bl cells were obtained through the NIH AIDS Research and Reference Reagent Program. Plasmid encoding SHIV.A.BG505 (42) was kindly provided by George Shaw of the University of Pennsylvania. N6-LS-WT (44) was kindly provided by John Mascola of NIH.

Humanized Mice. Generation of humanized mice was achieved as previously reported (34). Briefly, NSG (NOD.Cg-*Prkdc*^{scid} *Il2rg*^{tm1Wjl}/SzJ) mice were obtained from The Jackson Laboratory. Newborns between day 1 and day 5 were irradiated with 100 rad and then injected intrahepatically with 0.2×10^6 human hematopoietic CD34$^+$ stem cells 6 h later. The level of human engraftment was assessed 8 wk after transplantation. When humanization had occurred, the mice were infected by HIV-$1_{JR\text{-}CSF}$ or HIV-$1_{pNL(AD8)}$ via i.p. injection using a dose of 75,000 $TCID_{50}$. Plasma viral loads were monitored every week for 4 wk until the antibody experiments. All mice were bred and maintained at the Comparative Bioscience Center of The Rockefeller University in accordance with the regulations of its Institutional Animal Committee Care and Use Committee. These mouse studies were conducted under protocols approved by this committee.

Rhesus Macaques. Indian origin outbred adult rhesus monkeys (*Macaca mulatta*) screened for absence of class I alleles Mamu-A*01, Mamu-B*08, and Mamu-B*17 were used in this study. Groups were balanced for susceptible and resistant TRIM5α alleles (*SI Appendix*, Table S2). A total of 12 monkeys was infected with SHIV.A.BG505 (50 ng p27; 1.55×10^9 RNA copies) by the i.v. route, followed by weekly sampling of plasma viral load for 8 wk until the antibody experiment. All studies were approved by the Institutional Animal Care and Use Committee of the Tulane National Primate Research Center. Animal handling was carried out when the macaques were anesthetized with tiletamine/zolazepam (Telazol; 8 mg/kg) or ketamine-HCl (10 mg/kg).

Antibodies. All 117/1,400 antibody variants (WT, Null, and GASDALIE), 10E8.2/iMab and N6-LS-Null used in the humanized mouse experiments were generated in-house as previously described (34). Briefly, antibody-encoding DNA plasmids were transiently transfected into Expi293 cells (Life Technologies) using a 1:1:1:1 ratio by mass of the heavy-chain and light-chain plasmids encoding either arm of the bispecific antibodies, or a 1:1 ratio by mass of the heavy-chain and light-chain plasmids of N6-LS-Null. IgG was purified from supernatant using rProtein A Sepharose Fast Flow (GE Healthcare). The 117/1,400 variants (WT and Null) and 10E8.4/iMab used in rhesus macaques were produced by Wuxi Biologics, Inc. Size exclusion chromatography was used to assess physicochemical homogeneity of the test antibodies. Fifty μg of the antibodies were analyzed using an AKTA purifier FPLC (GE Healthcare) with column, flow rate, and mobile phase previously described (50).

Quantification of HIV-1 in Mouse Plasma by RT-PCR. Plasma HIV-1 RNA in humanized mice was quantified as previously reported (34, 51) with some modifications. RNA was extracted from 20 μL of plasma using the MinElute Virus Spin Kit (Qiagen) and then eluted. RT-PCR was performed in one step in a 30 μL reaction containing 10 μL of RNA, 1 × TaqMan PCR mix, 1 × TaqMan RT-enzyme mix (TaqMan RNA-to-Ct 1-Step Kit, Life Technologies), and primers/probe targeting a conserved region of the *pol* gene (forward primer 5′-CAATGGCAGCAATTTCACCA-3′; reverse primer 5′-GAATGCCAAATTCCTGCTTGA-3′; and probe 5′-HEX/CCCACCAAC/ZEN/AGGCGGCCTTAACTG/3IABkFQ-3′). Cycling conditions were 15 min at 48 °C, 17 min at 94 °C, followed by 50 cycles at 95 °C for 30 s and 60 °C for 60 s. Samples were run in duplicate in a 7,500 fast real-time PCR System (Applied Biosystems), and the limit of detection was 1,000 copies per milliliter of plasma.

Quantification of SHIV in Monkey Plasma by RT-PCR. Plasma SHIV RNA in rhesus macaques was quantified as previously reported (52). Briefly, plasma (1.5 mL) was centrifuged at ≥18,000 *g* for, at least, 1 h at 4 °C to pellet viruses. RNA was extracted from the pellets using the QIAamp Viral RNA Mini kit (Qiagen) as per the manufacturer's instructions. Viral RNA was reverse transcribed in 30 μL reactions containing 1 × TaqMan Buffer A (containing 50 mM KCl, 10 mM Tris·HCl, pH 8.3, 10 μM ethylenediaminetetraacetic acid [EDTA], 60 nM passive reference ROX) with 4.2 mM $MgCl_2$, 333 μM of each 2′-deoxynucleoside 5′-triphosphate (dNTP), 1.67 μM random hexamer, 20 U RNAsin (Promega), and 20 U SuperScript II reverse transcriptase (Life Technologies). Cycling conditions were 10 min at 25 °C, 50 min at 42 °C, and 10 min at 85 °C. Real-time PCR was performed by adding 20 μL of master mix to complementary DNA (cDNA) for a final volume of 50 μL containing a final concentration of 50 mM KCl, 10 mM Tris·HCl, pH 8.3, 10 μM EDTA, 60 nM passive reference ROX, 2.5 mM $MgCl_2$, 200 μM of each dNTP, 400 nM forward primer (gag-3.2: 5′-TGGAGAACAAAGAAGGATGTCAAA-3′), 400 nM reverse primer (gag-5.2: 5′-CACCAGATGACGCAGACAGTATTAT-3′), 100 nM probe (Gag-Btaq.2: 56-FAM/TTGGCACTA/ZEN/ATGGAGCTAAGACCGAAAGTATT/3IABkFQ), and 1.25 U AmpliTaq Gold (Life Technologies). Real-time PCR was run using Mx3000P (Stratagene) with the conditions of 95 °C for 10 min, followed by 55 cycles of 95 °C for 15 s and 60 °C for 50 s. Duplicate samples were analyzed and the limit of quantification was 12 SHIV RNA copies per milliliter of plasma.

Quantification of Cell-Associated SHIV RNA in Monkey PBMCs. To quantify cell-associated SHIV RNA, RNA was isolated from PBMCs using the RNeasy Plus Mini Kit (Qiagen), and RNA was first reverse transcribed into cDNA as described above. SHIV RNA was measured with a nested real-time PCR. The *gag* sequence was first preamplified using 200 nM of outer primers (5′outer: 5′-ACCCGGCGGAAAGAAAAAG-3′ and 3′outer: 5′-AATGCACCAGATGACGCAG-3′). The cycling conditions were 5 min at 95 °C, followed by 15 cycles at 95 °C for 30 s, 55 °C for 30 s, and 72 °C for 1 min. The amplified product was then used for nested PCR with the same primer/probe and PCR conditions described above for SHIV viral load, and 18S ribosomal RNA copy was quantified for each sample in parallel to normalize the cellular input with the same RT-PCR conditions for the SHIV viral load except using different primer/probes (18S forward: 5′-CCATGAACGAGGAATTCCCAGTAA-3′, 18S reverse: 5′- CCTCACTAAACCATCCAATCGGTAGTA-3′, and 18S probe: 5HEX/TAATCAACG/ZEN/CAAGCTTATGACCCGCACT/3IABkFQ).

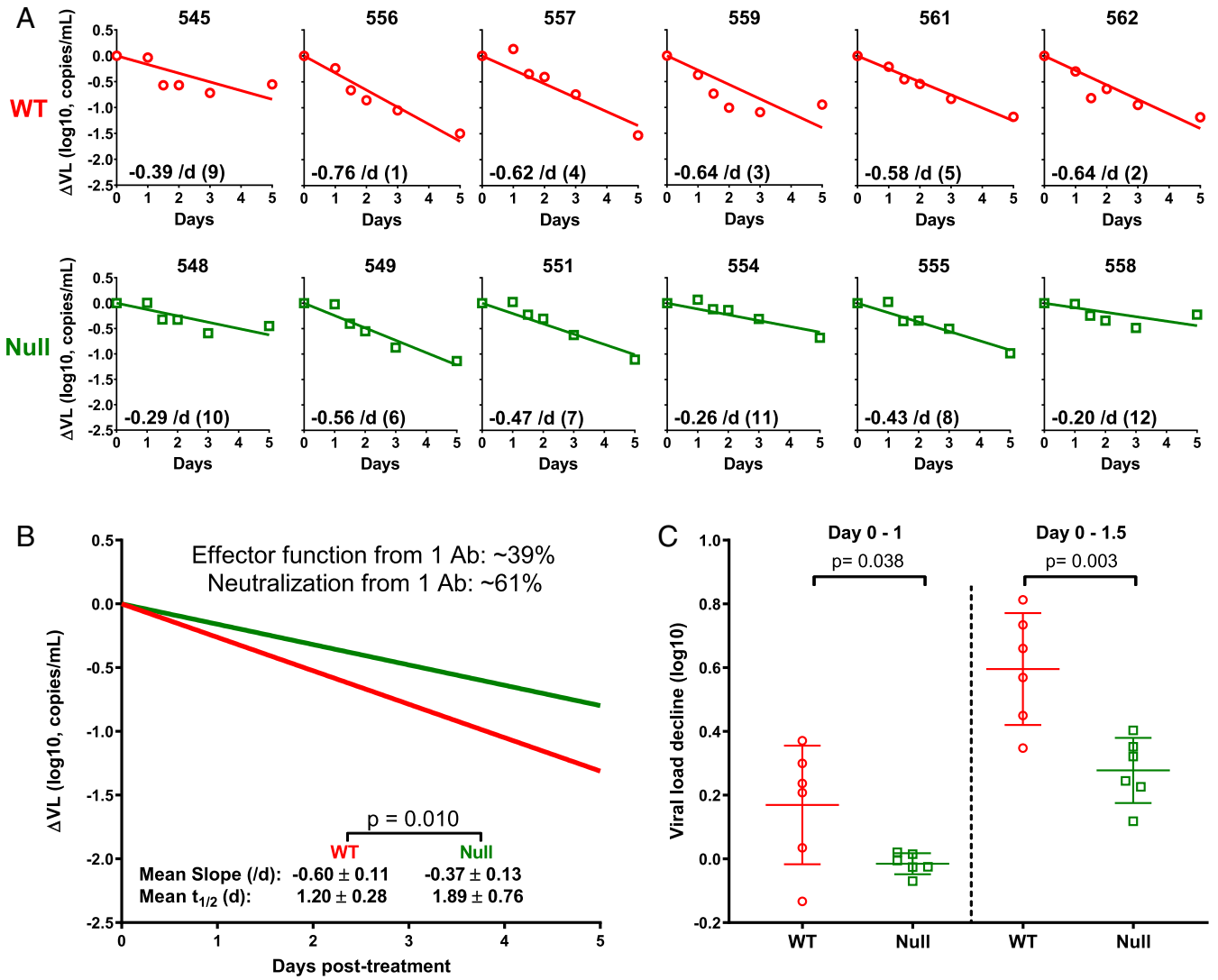

Fig. 4. Measuring and analyzing the plasma ΔVL in humanized mice infected with a different HIV-1 strain and treated with a different antibody. (*A*) HIV-$1_{pNL(AD8)}$–infected humanized mice were treated with N6-LS-WT (red) or N6-LS-Null (green). Plasma ΔVL is shown for each mouse. (*B*) Mean decay slopes on a natural log scale for the WT and Null groups. (*C*) Magnitude of plasma ΔVL from day 0 to day 1 and day 0–1.5 postantibody treatment. Lines represent mean ± SD, and *P* values were calculated by a two-tailed *t* test.

Surface Plasmon Resonance. The binding of 117/1,400 and N6-LS variants to human or rhesus macaque FcγRs was detected by a Biacore T200 surface plasmon resonance system (GE Healthcare) as previously reported (18). All experiments were performed at 25 °C in HBS-EP+ buffer (10 mM 4-[2-hydroxyethyl]-1-piperazineethanesulfonic acid, pH 7.4; 150 mM NaCl; 3.4 mM EDTA; 0.005% [vol/vol] surfactant P20). Human FcγRIIa, FcγRIIb, and FcγRIIIa and rhesus FcγRIIa and FcγRIIIa, diluted at 20 μg/mL in 10 mM sodium acetate, pH 4.5 (or pH 5.0 for human FcγRIIb) were immobilized on Series S CM5 chips by amine coupling, resulting in a density of 2,000 response units. Antibodies were injected through flow cells at different concentrations (ranging from 4,000 to 31.25 nM in 1:2 successive dilutions) at a flow rate of 30 μL/min for 120 s, followed by a 300 s dissociation step. After each assay cycle, the sensor surface was regenerated with a 30 s injection of 25 mM NaOH at a flow rate of 30 μL/min. Background binding to blank immobilized flow cells was subtracted, and sensograms of antibodies binding to FcγRs were generated using Biacore T200 evaluation software (GE Healthcare) with the 1:1 Langmuir binding model.

Quantification of Plasma Anti–HIV-1 IgG Levels by Enzyme-Linked immunosorbent Assay. Antibody levels in plasma (10E8.2/iMab, 117/1,400 variants, and N6-LS variants in mouse plasma and 10E8.4/iMab and 117/1,400 variants in rhesus macaque plasma) were measured using an enzyme-linked immunosorbent assay (ELISA) as previously reported (34) with some modifications. CoStar 96-well EIA/RIA plates (Corning) were coated with 20 ng or 100 ng of soluble CD4 or HIV-1 gp120 protein (Sino Biologics) per well and incubated overnight at 4 °C. Plates were washed three times with phosphate-buffered saline (PBS) + 0.05% (vol/vol) Tween-20 (PBST) and blocked with PBS containing 5% (wt/vol) milk and 0.5% (wt/vol) bovine serum albumin (BSA) for 2 h at room temperature. Plasma samples were inactivated by incubating in 1% (vol/vol) Triton X-100 (Sigma-Aldrich). Serial dilutions of inactivated plasma prepared in PBS containing 2% (wt/vol) milk, and 0.2% (wt/vol) BSA were then added on to the coated plates in duplicates and incubated for 2 h. Respective triton-inactivated antibodies were used in duplicate for the standard curve. After washing, peroxidase-conjugated goat anti-human IgG (Jackson ImmunoResearch) for mouse plasma, or horseradish peroxidase (HRP)-conjugated goat anti-human IgG (monkey adsorbed, Bethyl Laboratories) for monkey plasma, was incubated for 1 h at room temperature. For detection of 10E8.4/iMab in monkey plasma, 50 ng per well 10E8.4/iMab anti-idiotype antibody (Syngene) was added prior to the addition of HRP-conjugated goat anti-mouse cross-absorbed IgG (ThermoFisher Scientific). Samples were detected by a tetramethylbenzidine (TMB) liquid substrate system (Sigma-Aldrich), and spectrophotometric readings were performed at 450 nm. The limit of detection for the assay was 0.1 μg/mL.

Detection of Anti-117/1,400 or anti-10E8.4/iMab Antibody Titer in Rhesus Macaques. Anti-117/1,400 or anti-10E8.4/iMab antibody titers in macaque plasma were measured by ELISA. CoStar 96-well EIA/RIA plates were coated overnight with 50 ng of the 117/1,400 variant or 10E8.4/iMab antibody.

Plates were washed with PBST and blocked with PBS containing 5% milk and 0.5% BSA for 2 h at room temperature. Macaque plasma was inactivated by incubating in 1% Triton X-100. Serial dilutions of inactivated plasma prepared in PBS containing 2% milk and 0.2% BSA were then added onto the coated plate in duplicates and incubated for 2 h. After washing, HRP-conjugated mouse anti-rhesus IgG (human antibody preabsorbed, Abcam) was added and incubated for 1 h at room temperature. Samples were detected by a TMB liquid substrate system, and spectrophotometric readings were performed at 450 nm. Negative values were graphed with a titer of 25, which is half of the lowest dilution tested (1:50).

In Vitro Neutralization of HIV-1. In vitro neutralizing activity of antibodies was tested against a panel of 118 multiclade HIV-1 envelope pseudoviruses, HIV-$1_{JR\text{-}CSF}$, HIV-$1_{pNL(AD8)}$, or SHIV.A.BG505 as previously described (53). Serial dilutions of antibodies were incubated with the viruses and added to TZM-bl cells carrying a luciferase reporter gene. Following a 48-h incubation, cells were lysed, and luciferase activity was measured. Concentration that inhibits response by 50% values reflect the amount of antibody sufficient to reduce luciferase activity by 50%.

Statistics. Differences in viral-load/CA-RNA decay slopes among treatment groups were assessed by the Mann–Whitney test. For the antibody PK studies, data points represent the mean plasma concentrations of different treatment groups at each time point indicated, and the error bars represent SD.

Data Availability. All the data and materials supporting this study are shown in the main text figures and *SI Appendix*.

ACKNOWLEDGMENTS. We thank Chris Chen and colleagues at Wuxi Biologics for large-scale production of antibodies for monkey experiments, Michael Seaman for virus neutralization data, George Shaw for providing SHIV.A.BG505, John Mascola for providing N6-LS, and Stanca Ciupe for data analysis. This work was supported by NIH Grants RO1-AI145645 (to D.D.H.), RO1-AI129802 (to D.D.H.), RO1-AI134328 (to D.D.H.), DP1-DA0333263 (to D.D.H.), RO1-AI028433 (to A.S.P.), RO1-OD011095 (to A.S.P.), and PO1-AI131365 (to A.S.P.), as well as by Grants OPP1169162 (to D.D.H.) and OPP1040731 (to D.D.H.) from the Bill & Melinda Gates Foundation. Portions of this work were also performed under the auspices of US Department of Energy Contract 89233218CNA000001 (to A.S.P.).

1. L. L. Lu, T. J. Suscovich, S. M. Fortune, G. Alter, Beyond binding: Antibody effector functions in infectious diseases. *Nat. Rev. Immunol.* **18**, 46–61 (2018).
2. S. Bournazos, J. V. Ravetch, Anti-retroviral antibody FcγR-mediated effector functions. *Immunol. Rev.* **275**, 285–295 (2017).
3. X. Wang, M. Mathieu, R. J. Brezski, IgG Fc engineering to modulate antibody effector functions. *Protein Cell* **9**, 63–73 (2018).
4. M. Kramski, M. S. Parsons, I. Stratov, S. J. Kent, HIV-specific antibody immunity mediated through NK cells and monocytes. *Curr. HIV Res.* **11**, 388–406 (2013).
5. W. Wang, A. K. Erbe, J. A. Hank, Z. S. Morris, P. M. Sondel, NK cell-mediated antibody-dependent cellular cytotoxicity in cancer immunotherapy. *Front. Immunol.* **6**, 368 (2015).
6. C. Stein, I. Schubert, G. H. Fey, Natural killer (NK)-and T-cell engaging antibody-derived therapeutics. *Antibodies (Basel)* **1**, 88–123 (2012).
7. D. J. DiLillo, G. S. Tan, P. Palese, J. V. Ravetch, Broadly neutralizing hemagglutinin stalk-specific antibodies require FcγR interactions for protection against influenza virus in vivo. *Nat. Med.* **20**, 143–151 (2014).
8. B. M. Gunn *et al*., A role for Fc function in therapeutic monoclonal antibody-mediated protection against Ebola virus. *Cell Host Microbe* **24**, 221–233.e5 (2018).
9. E. O. Saphire *et al*., Systematic analysis of monoclonal antibodies against Ebola virus GP defines features that contribute to protection. *Cell* **174**, 938–952.e13 (2018).
10. A. J. Hessell *et al*., Fc receptor but not complement binding is important in antibody protection against HIV. *Nature* **449**, 101–104 (2007).
11. D. R. Burton *et al*., A large array of human monoclonal antibodies to type 1 human immunodeficiency virus from combinatorial libraries of asymptomatic seropositive individuals. *Proc. Natl. Acad. Sci. U.S.A.* **88**, 10134–10137 (1991).
12. P. W. Parren *et al*., Antibody protects macaques against vaginal challenge with a pathogenic R5 simian/human immunodeficiency virus at serum levels giving complete neutralization in vitro. *J. Virol.* **75**, 8340–8347 (2001).
13. D. R. Burton *et al*., Efficient neutralization of primary isolates of HIV-1 by a recombinant human monoclonal antibody. *Science* **266**, 1024–1027 (1994).
14. B. Moldt *et al*., A panel of IgG1 b12 variants with selectively diminished or enhanced affinity for Fcγ receptors to define the role of effector functions in protection against HIV. *J. Virol.* **85**, 10572–10581 (2011).
15. M. S. Parsons *et al*., Fc-dependent functions are redundant to efficacy of anti-HIV antibody PGT121 in macaques. *J. Clin. Invest.* **129**, 182–191 (2019).
16. A. Halper-Stromberg *et al*., Broadly neutralizing antibodies and viral inducers decrease rebound from HIV-1 latent reservoirs in humanized mice. *Cell* **158**, 989–999 (2014).
17. J. F. Scheid *et al*., Sequence and structural convergence of broad and potent HIV antibodies that mimic CD4 binding. *Science* **333**, 1633–1637 (2011).
18. S. Bournazos *et al*., Broadly neutralizing anti-HIV-1 antibodies require Fc effector functions for in vivo activity. *Cell* **158**, 1243–1253 (2014).
19. C. L. Lu *et al*., Enhanced clearance of HIV-1-infected cells by broadly neutralizing antibodies against HIV-1 in vivo. *Science* **352**, 1001–1004 (2016).
20. L. H. Wren *et al*.; ADCC study collaboration investigators, Specific antibody-dependent cellular cytotoxicity responses associated with slow progression of HIV infection. *Immunology* **138**, 116–123 (2013).
21. L. L. Baum *et al*., HIV-1 gp120-specific antibody-dependent cell-mediated cytotoxicity correlates with rate of disease progression. *J. Immunol.* **157**, 2168–2173 (1996).
22. A. W. Chung *et al*., Activation of NK cells by ADCC antibodies and HIV disease progression. *J. Acquir. Immune Defic. Syndr.* **58**, 127–131 (2011).
23. O. Lambotte *et al*., Heterogeneous neutralizing antibody and antibody-dependent cell cytotoxicity responses in HIV-1 elite controllers. *AIDS* **23**, 897–906 (2009).
24. B. F. Haynes *et al*., Immune-correlates analysis of an HIV-1 vaccine efficacy trial. *N. Engl. J. Med.* **366**, 1275–1286 (2012).
25. G. D. Tomaras *et al*., Vaccine-induced plasma IgA specific for the C1 region of the HIV-1 envelope blocks binding and effector function of IgG. *Proc. Natl. Acad. Sci. U.S.A.* **110**, 9019–9024 (2013).
26. X. Wei *et al*., Viral dynamics in human immunodeficiency virus type 1 infection. *Nature* **373**, 117–122 (1995).
27. D. D. Ho *et al*., Rapid turnover of plasma virions and CD4 lymphocytes in HIV-1 infection. *Nature* **373**, 123–126 (1995).
28. M. Markowitz *et al*., A novel antiviral intervention results in more accurate assessment of human immunodeficiency virus type 1 replication dynamics and T-cell decay in vivo. *J. Virol.* **77**, 5037–5038 (2003).
29. B. Ramratnam *et al*., Rapid production and clearance of HIV-1 and hepatitis C virus assessed by large volume plasma apheresis. *Lancet* **354**, 1782–1785 (1999).
30. A. S. Perelson, P. Essunger, D. D. Ho, Dynamics of HIV-1 and CD4+ lymphocytes in vivo. *AIDS* **11**, S17–S24 (1997).
31. A. S. Perelson *et al*., Decay characteristics of HIV-1-infected compartments during combination therapy. *Nature* **387**, 188–191 (1997).
32. A. S. Perelson, A. U. Neumann, M. Markowitz, J. M. Leonard, D. D. Ho, HIV-1 dynamics in vivo: Virion clearance rate, infected cell life-span, and viral generation time. *Science* **271**, 1582–1586 (1996).
33. D. Sok *et al*., Recombinant HIV envelope trimer selects for quaternary-dependent antibodies targeting the trimer apex. *Proc. Natl. Acad. Sci. U.S.A.* **111**, 17624–17629 (2014).
34. Y. Huang *et al*., Engineered bispecific antibodies with exquisite HIV-1-neutralizing activity. *Cell* **165**, 1621–1631 (2016).
35. E. Arduin *et al*., Highly reduced binding to high and low affinity mouse Fc gamma receptors by L234A/L235A and N297A Fc mutations engineered into mouse IgG2a. *Mol. Immunol.* **63**, 456–463 (2015).
36. V. Oganesyan, C. Gao, L. Shirinian, H. Wu, W. F. Dall'Acqua, Structural characterization of a human Fc fragment engineered for lack of effector functions. *Acta Crystallogr. D Biol. Crystallogr.* **64**, 700–704 (2008).
37. D. J. DiLillo, J. V. Ravetch, Differential Fc-receptor engagement drives an anti-tumor vaccinal effect. *Cell* **161**, 1035–1045 (2015).
38. T. Strowig *et al*., Human NK cells of mice with reconstituted human immune system components require preactivation to acquire functional competence. *Blood* **116**, 4158–4167 (2010).
39. P. M. Hogarth, J. C. Anania, B. D. Wines, The FcγR of humans and non-human primates and their interaction with IgG: Implications for induction of inflammation, resistance to infection and the use of therapeutic monoclonal antibodies. *Curr. Top. Microbiol. Immunol.* **382**, 321–352 (2014).
40. A. M. Chenoweth, H. M. Trist, P. S. Tan, B. D. Wines, P. M. Hogarth, The high-affinity receptor for IgG, FcγRI, of humans and non-human primates. *Immunol. Rev.* **268**, 175–191 (2015).
41. A. W. Boesch, A. R. Miles, Y. N. Chan, N. Y. Osei-Owusu, M. E. Ackerman, IgG Fc variant cross-reactivity between human and rhesus macaque FcγRs. *MAbs* **9**, 455–465 (2017).
42. H. Li *et al*., Envelope residue 375 substitutions in simian-human immunodeficiency viruses enhance CD4 binding and replication in rhesus macaques. *Proc. Natl. Acad. Sci. U.S.A.* **113**, E3413–E3422 (2016).
43. N. N. Padte, J. Yu, Y. Huang, D. D. Ho, Engineering multi-specific antibodies against HIV-1. *Retrovirology* **15**, 60 (2018).
44. J. Huang *et al*., Identification of a CD4-binding-site antibody to HIV that evolved near-Pan neutralization breadth. *Immunity* **45**, 1108–1121 (2016).
45. P. W. Denton *et al*., Targeted cytotoxic therapy kills persisting HIV infected cells during ART. *PLoS Pathog.* **10**, e1003872 (2014).
46. E. Brandin, R. Thorstensson, S. Bonhoeffer, J. Albert, Rapid viral decay in simian immunodeficiency virus-infected macaques receiving quadruple antiretroviral therapy. *J. Virol.* **80**, 9861–9864 (2006).
47. M. A. Nowak *et al*., Viral dynamics of primary viremia and antiretroviral therapy in simian immunodeficiency virus infection. *J. Virol.* **71**, 7518–7525 (1997).
48. T. W. North *et al*., Enhanced antiretroviral therapy in rhesus macaques improves RT-SHIV viral decay kinetics. *Antimicrob. Agents Chemother.* **58**, 3927–3933 (2014).
49. C. P. Kalberer, U. Siegler, A. Wodnar-Filipowicz, Human NK cell development in NOD/SCID mice receiving grafts of cord blood CD34+ cells. *Blood* **102**, 127–135 (2003).
50. C. S. Pace *et al*., Bispecific antibodies directed to CD4 domain 2 and HIV envelope exhibit exceptional breadth and picomolar potency against HIV-1. *Proc. Natl. Acad. Sci. U.S.A.* **110**, 13540–13545 (2013).
51. F. Klein *et al*., HIV therapy by a combination of broadly neutralizing antibodies in humanized mice. *Nature* **492**, 118–122 (2012).
52. C. D. Andrews *et al*., Long-acting integrase inhibitor protects macaques from intrarectal simian/human immunodeficiency virus. *Science* **343**, 1151–1154 (2014).
53. M. S. Seaman *et al*., Tiered categorization of a diverse panel of HIV-1 Env pseudoviruses for assessment of neutralizing antibodies. *J. Virol.* **84**, 1439–1452 (2010).